Check for updates

RESEARCH ARTICLE

Functional Ecology | BRITISH ECOLOGICAL SOCIETY

Foraging under extreme events: Contrasting adaptations by benthic macrofauna to drastic biogeochemical disturbance

Yiming V. Wang[1,2] | **Thomas Larsen**[1] | **Mario Lebrato**[2] | **Li-Chun Tseng**[3] | **Pei-Wen Lee**[3] | **Nicolás Sánchez**[4] | **Juan-Carlos Molinero**[5] | **Jiang-Shiou Hwang**[3,6,7] | **Tin-Yam Chan**[3,6] | **Dieter Garbe-Schönberg**[2]

[1]Max Planck Institute of Geoanthropology, Jena, Germany; [2]Institute of Geosciences, Kiel University, Kiel, Germany; [3]Institute of Marine Biology, National Taiwan Ocean University, Keelung, Taiwan; [4]GEOMAR Helmholtz Centre for Ocean Research Kiel, Kiel, Germany; [5]MARBEC - Marine Biodiversity, Exploitation and Conservation, IRD/CNRS/IFREMER/Univ Montpellier, Sète Cedex, France; [6]Center of Excellence for the Oceans, National Taiwan Ocean University, Keelung, Taiwan and [7]Center of Excellence for Ocean Engineering, National Taiwan Ocean University, Keelung, Taiwan

Correspondence

Yiming V. Wang
Email: ywang@shh.mpg.de

Handling Editor: Rana El-Sabaawi

Abstract

1. Hydrothermal vent systems are important biodiversity hotspots that host a vast array of unique species and provide information on life's evolutionary adaptations to extreme environments. However, these habitats are threatened by both human exploitation and extreme natural events, both of which can rapidly disrupt the delicate balance of the food webs found in these systems. This is particularly true for shallow vent endemic animals due to their limited dietary niche and specialized adaptations to specific biogeochemical conditions.

2. In this study, we used the shallow hydrothermal vents of Kueishantao off the coast of Taiwan as a natural laboratory to examine the response of a benthic food web to a M5.8 earthquake and a C5 typhoon that led to a two-year "near shutdown" of the vents. These perturbations drastically altered the local biogeochemical cycle and the dietary availability of chemosynthetic versus photosynthetic food resources.

3. Our analysis of multiple stable isotopes, including those of sulphur, carbon, and nitrogen (δ^{34}S, δ^{13}C, and δ^{15}N), from different benthic macrofauna reveals that endemic and non-endemic consumers exhibited different responses to sudden disruption in habitat and biogeochemical cycling.

4. The endemic vent crab, *Xenograpsus testudinatus*, continued to partially rely on chemosynthetic sulphur bacteria despite photosynthetic sources being the most dominant food source after the disruption. We posit that *X. testudinatus* has an obligate nutritional dependence on chemoautotrophic sources because the decrease in chemoautotrophic production was accompanied by a dramatic decrease in the abundance of *X. testudinatus*. The population decline rate was ~19 individuals per m² per year before the perturbation, but the decline rate increased to 40

individuals per m^2 per year after the perturbation. In contrast, the non-endemic gastropods exhibited much greater dietary plasticity that tracked the overall abundance of photo- and chemo-synthetic dietary sources.

5. The catastrophic events in shallow hydrothermal vent ecosystem presented a novel opportunity to examine dietary adaptations among endemic and non-endemic benthic macrofauna in response to altered biogeochemical cycling. Our findings highlight the vulnerability of benthic specialists to the growing environmental pressures exerted by human activities worldwide.

1 | INTRODUCTION

Marine ecosystems and biogeochemical cycles are facing growing pressures from extreme natural events and human activities, resulting in a rapid loss of biodiversity and changes to the functioning of food webs (Rees, 2012). This is particularly true for benthic food webs, which are often spatially fragmented and inhabited by rare, endangered, or endemic faunal species (Ashford et al., 2019; Gianni et al., 2016). Gaining a better understanding of how benthic communities respond to sudden and unpredictable disturbances is crucial for evaluating their resilience and vulnerability and for formulating effective conservation and management strategies for these habitats. Monitoring such disturbances in most natural habitats is challenging (Hall-Spencer et al., 2008; Harada et al., 2020), and replicating large-scale environmental disturbances in controlled experiments presents its own set of challenges (Ledger et al., 2013; Sagarin et al., 2016). However, valuable insights into the response of benthic communities to disturbances can be obtained through longitudinal studies that take advantage of naturally occurring events in areas prone to earthquakes, typhoons, and other extreme disturbances. Shallow marine hydrothermal vents, also known as shallow vents, offer a unique opportunity to study benthic communities in response to such disturbances.

Benthic species in these chemosynthetic ecosystems rely on both chemosynthetic and photosynthetic resources (Ho et al., 2015; Reid et al., 2013; Tarasov et al., 2005; Wang et al., 2015). Chemosynthetic production occurs when warm vent fluids rich in sulphides, methane, and other minerals mix with seawater (Chan et al., 2016; Chen et al., 2017; Hall-Spencer et al., 2008; Levin et al., 2016; Tarasov et al., 2005). The availability of chemosynthetic and photosynthetic dietary resources is largely influenced by the intensity of the vent and its interaction with the surrounding ecosystem through horizontal and vertical transport pathways (Levin et al., 2016). These pathways are in turn affected by various factors, such as changes in vent fluid flow, elemental cycling, and seawater mixing (Levin et al., 2016; Ramirez-Llodra et al., 2011; Tarasov et al., 2005). Therefore, both chemosynthetic and photosynthetic producers fuelling these unique food webs are sensitive to perturbations.

The ability of vent animals to use chemosynthetic sources and tolerate high levels of toxicity, such as hydrogen sulphide (H$_2$S), makes them model species for understanding the origin of life on Earth (Little & Vrijenhoek, 2003; Luther et al., 2001; Martin et al., 2008; Minic, 2009; Petersen et al., 2011; Sellanes et al., 2011). Despite this importance, these chemosynthetic ecosystems are facing threats, including climate change, resource exploitation, and pollution (Levin et al., 2016; Ramirez-Llodra et al., 2011; Suzuki et al., 2018) and our understanding of how shallow marine chemosynthetic ecosystems respond to sudden and drastic biogeochemical disruptions is limited. These disruptions can alter the balance between chemosynthetic and photosynthetic primary production, potentially leading to dire consequences for consumer populations (Bell et al., 2017; Kharlamenko et al., 1995; Levin et al., 2016; Portail et al., 2016; Sellanes et al., 2011; Suzuki et al., 2018; Wu et al., 2021).

In 2016, one of the most studied shallow marine vent systems in the world, Kueishantao (KST), also known as Turtle Island off the coast of Taiwan, was hit by a M5.8 earthquake and a subsequent C5 typhoon within a few weeks (12 May and 2–10 July, respectively, Supporting Information Videos S1 and S2). KST is located at 24.843°N, 121.951°E with the depth of water <30 m. The site background information is detailed in Supporting Information Text I. These extreme events triggered underwater landslides, which buried active vents and benthic habitat and caused a near "shutdown" of vent activity for almost two years (Figure 1, Lebrato et al., 2019). The combined effect of earthquake and typhoon decreased the toxicity and intensity of the discharging shallow vent fluids (Lebrato et al., 2019), which are the two most important factors in structuring the food webs at KST (Chan et al., 2016; Chen et al., 2017). Before the extreme events, the active Yellow Vents (YV) and the semi-inactive White Vents (WV) at KST had distinct biogeochemical properties (Figure 2). The hot and toxic YV discharged gases and fluids rich in CO$_2$, hydrogen sulphide (H$_2$S) and sulphur dioxide (SO$_2$) (Chen et al., 2005). In contrast, the WV had low degassing activity and no
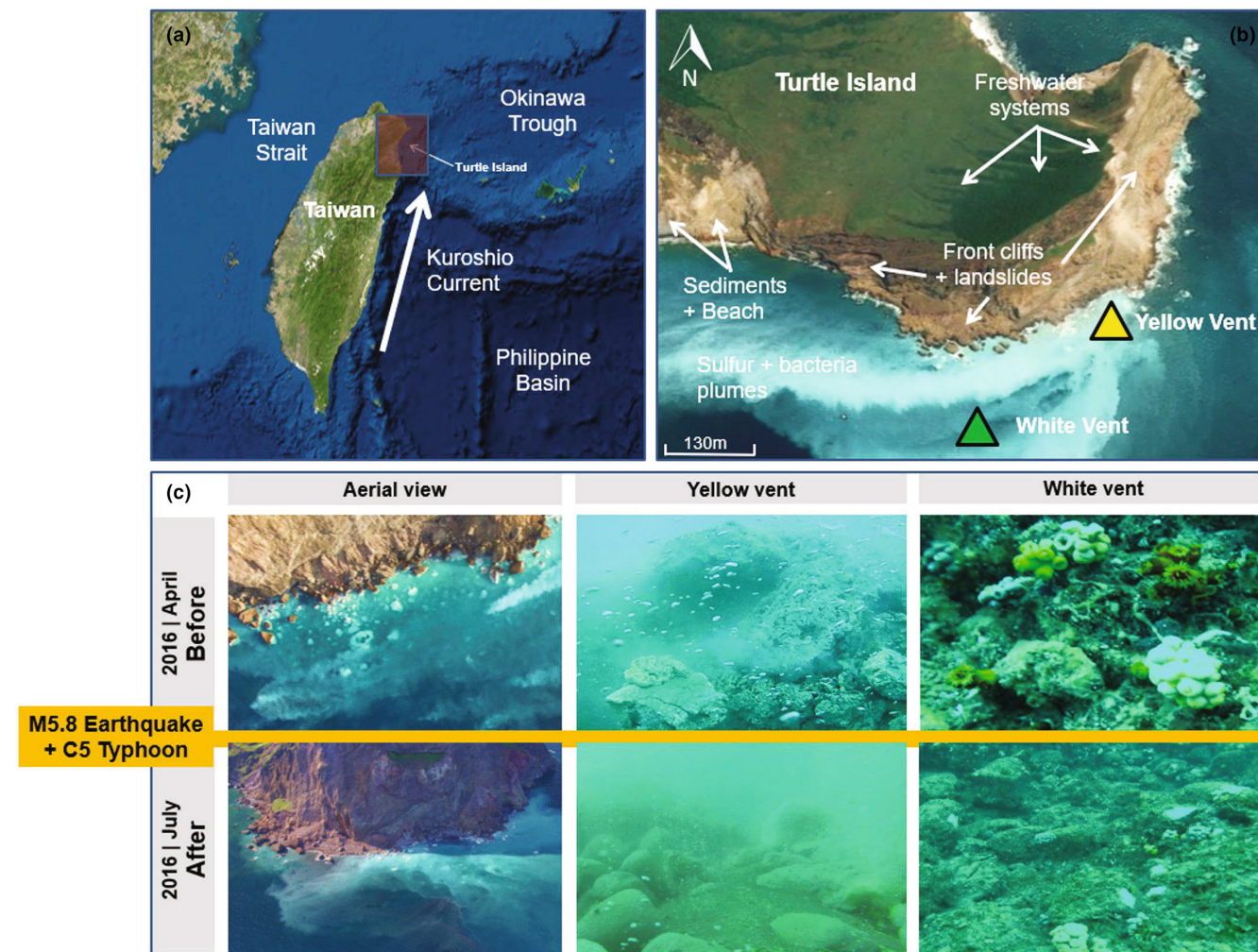
FIGURE 1 Geographic location of Kuishantao (Turtle Island, off Taiwan) and photographs showing the disturbance events that affected the activity of the shallow hydrothermal vents: (a) Shallow vents area, located at a tectonic junction northeast of Taiwan and at the southern end of the Okinawa trough. Its eastern side is directly hit by the Kuroshio current. (b) Sampling locations at the yellow vent (YV, water depth 6–10m), the white vent (WV, water depth 16–18m), and old vent sites, as well as details of the east side of Turtle Island. (c) Aerial and submarine photographs showing vent activity and seabed conditions at sampling sites before and after the 5.8 Richter magnitude earthquake on 12 May 2016, and the Category 5 typhoon Nepartak from 2 to 10 July 2016. Detailed time series aerial and submarine photos from 2011 to 2018 can be found in Lebrato et al. (2019).

discharge of toxic fluids (Chen et al., 2005; Supporting Information Text II). After the disturbance, the rapid change in the physical environment and the reduction in vent discharges led to dramatic changes in seawater biogeochemistry at both YV and WV (Lebrato et al., 2019). Specifically, a significant reduction in venting activity and fluid flow was observed at YV along with a complete depletion of dissolved elements (e.g., Cd, Ba, Pb, Fe, Cu, As, Cl, and Mg), which recovered to pre-disturbance concentrations 2 years later (Lebrato et al., 2019). Most notably, previously abundant native yellow sulphur accretions near the active YV completely disappeared for 2 years (Figure 1c). Time series of drone images in the region (Supporting Information Text II and Supporting Information Video S3) show a noticeable decline in the vibrant hue generated by the prevalent chemoautotrophic sulphur bacteria (e.g., epsilonproteobacteria and gammaproteobacteria) in the WV seawater after the extreme events

(Lebrato et al., 2019). This reduction in chemosynthetic activity may have caused a shift in the benthic food source from chemosynthetic to photosynthetic resources.

The only macrofaunal species (i.e., body length 0.5–50mm) to inhabit the hostile YV environment is the endemic vent crab *Xenograpsus testudinatus* (Ng et al., 2000). Its successful existence in the YV has been attributed to its unique physiological adaptation to highly acidic and toxic hydrothermal fluids (Chan et al., 2016; Hu et al., 2012; Yang et al., 2016). To date, it is unclear whether these highly adapted vent crabs are obligate feeders of sulphur bacteria because vent particulate organic matter (POM) can make up a substantial proportion (6%–87%) of their diet (Chang et al., 2018). The species is also known to opportunistically use photosynthetically derived foods (Chang et al., 2018; Ho et al., 2015; Jeng et al., 2004; Wang et al., 2014). For example, *X. testudinatus* feeds on a vast array
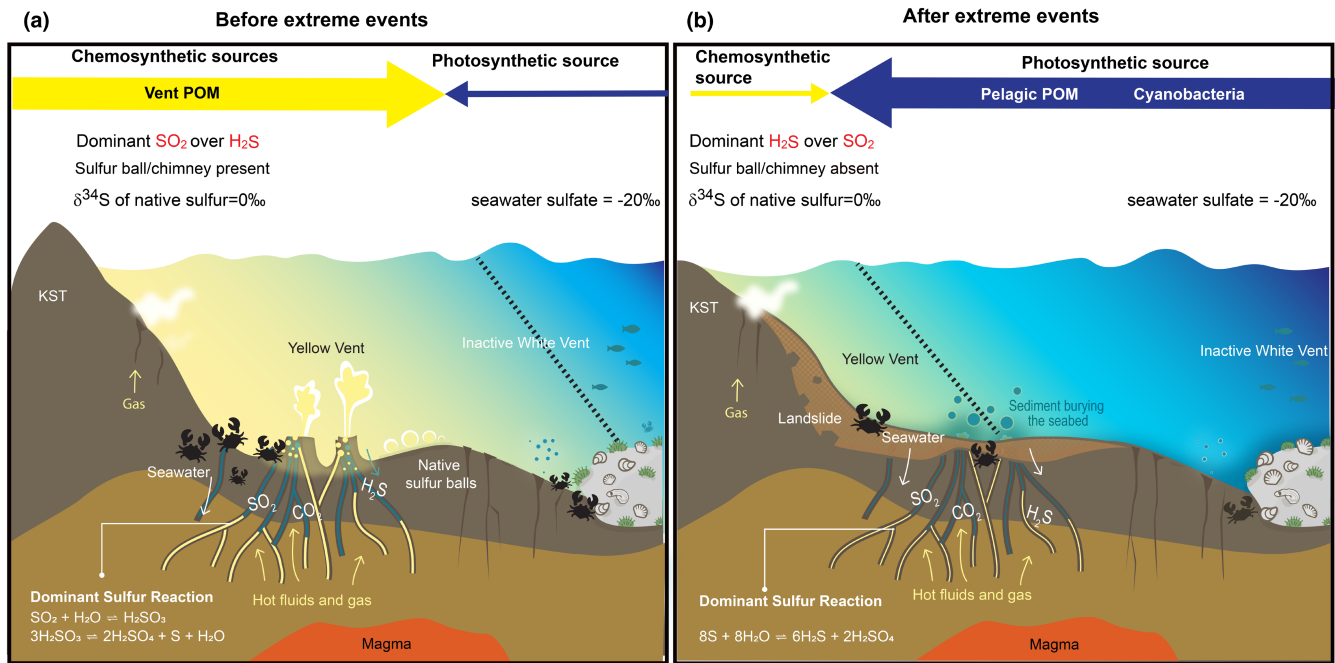
FIGURE 2 Conceptual framework diagram showing shifts in biogeochemical processes and dietary source mixing around Turtle Island shallow hydrothermal before and after the extreme events: (a) Prevailing contribution from chemosynthetic sources but minor contribution from photosynthetic sources before disturbance. Under this scenario, the POM input from the vent was strong in the vent area. Dominant sulphur reactions result in an oxidizing state with a more dominant SO_2/H_2S ratio, leading to precipitation and formation of a bright yellow sulphur element chimney and balls at the Yellow Vents. (b) Prevailing contribution from photosynthetic sources but minor contribution from the chemosynthetic source after the disturbance. Under this scenario, the vent POM decreased drastically, while the seawater POM became the dominant basal resource in the vent area. The disappearance of previously abundant native yellow sulphur accretions on the seafloor near the active YV is a result of changes in sulphur speciation from an oxidizing state to a reductive state (decreasing ratio of SO_2 to H_2S). This has resulted in ^{34}S depletion of overall sulphur species in the KST vent fluids (Galkin & Sagalevich, 2017). In addition to sulphur speciation, there was a major reduction in sulphur fluid fluxes at the YV, leading to the increased influence of seawater (more ^{34}S enriched) in the mixing zone. Figure created by Michelle O'Reilly from the Max Planck Institute of Geoanthropology, Jena, Germany.

of zooplankton that are killed by the sulphurous plumes of the vents during slack water episodes (Jeng et al., 2004). Gut content analyses show that the species also feeds on detritus and biofilms on vent rocks (Wang et al., 2014). Compared to the YV, the less hostile WV has much higher faunal diversity (Figure 2). Besides the endemic *X. testudinatus*, the WV hosts numerous generalist species such as gastropods (e.g., sessile species *Bostrycapulus gravispinosus*, *Thylacodes adamsii*, mobile gastropods such as *Ergalatax contrata*) capable of rapidly colonizing early succession habitat and using a variety of resources (Chan et al., 2016). Vent-dwelling gastropods acquire most (60%–80%) of their diet from photosynthetic production (Chang et al., 2018). The coexistence of obligate and non-endemic vent species before and after the extreme events makes KST a valuable site for investigating how different members of benthic food webs respond to sudden and drastic changes in biogeochemical and physical conditions.

To understand how the changes in biogeochemical cycles triggered by the extreme events in 2016 altered the KST benthic food web, we sampled *X. testudinatus* and three generalist gastropod species in the peripheral WV area (Chan et al., 2016; Chen et al., 2017): the sessile snail *Thylacodes adamsii* (Mörch, 1859) and two mobile gastropods, the limpet *Bostrycapulus gravispinosus* (Kuroda & Habe,

1950) and the snail *Ergalatax contracta* (Reeve, 1846), in 2015 and 2018. These gastropods are pioneer species, abundant and fairly tolerant to toxic conditions (Chen et al., 2017). The feeding strategies of the three gastropods differ: *T. adamsii* and *B. gravispinosus* are filter feeders and *E. contracta* carnivorous (Chan et al., 2016; Chen et al., 2017). We analysed the stable isotopes of sulphur, carbon, and nitrogen ($\delta^{34}S$, $\delta^{13}C$, and $\delta^{15}N$) of consumers and their potential food resources to understand the changes in diet. Sulphur is a powerful tracer for distinguishing between hydrothermal chemosynthetic and photosynthetic resources. Chemosynthetic production generally has lower $\delta^{34}S$ values than photosynthetic production (Fry, 1988; Fry et al., 1983, 1991). As for carbon, $\delta^{13}C$ values are generally lower for chemo- than photosynthetic production, because more reductive conditions allow methane to be used as a source of carbon and energy (Wang et al., 2018). However, it is also important to consider that sulphur oxidizers partially rely on the reductive tricarboxylic acid cycle (rTCA) for CO_2 fixation (Tang & Blankenship, 2010). This pathway discriminates less against ^{13}C than the otherwise dominant Calvin-Benson-Bassham cycle (Hügler & Sievert, 2011). This may explain why Chang et al. (2018) found that vent POM from KST area was more ^{13}C enriched than seawater POM (−18.2‰ vs. −23.4‰). Finally, $\delta^{15}N$ values are usually used as an indicator of trophic

position due to ^{15}N enrichment during trophic transfer (McCutchan Jr et al., 2003; Post, 2002). It is uncertain whether ^{15}N is diagnostic of chemo- or photosynthetic resources other than deep-sea hydrothermal vent fauna tend to have lower δ^{15}N values than deep-sea non-vent fauna (Michel et al., 2021). Given the close association of *X. testudinatus* with shallow hydrothermal vent systems, we hypothesize that this endemic species will be more sensitive to a decrease in chemosynthetic production than generalist species.

2 | MATERIALS AND METHODS

2.1 | Sampling and processing

No sample permits were required for our fieldwork. Research cruises for the collection of vent organisms were carried out between April and May each year in 2015 and 2018 to avoid seasonal variation of photosynthetic production, which can be influenced by seawater temperature and the direction of the predominant tides and the Kuroshio Current. After the extreme events, the YV landscape was fragmented due to landslides on the shore. The accumulated YV sulphur chimney was completely destroyed and the original seabed landscape was buried with new layers of debris and sediments. Vent activities in the YV increased again in 2018 in many smaller fumaroles. Hence, the sampling in 2018 was conducted on top of the old buried YV site, located through GPS and other landmarks. The WV seabed (16–18 m), located farther away from the shoreline (6–10 m), was buried with only a thin layer of sediment and had less venting activity in 2018 compared to 2015, allowing us to sample the same site in the WV in 2018.

Vent organisms were collected around the same transect on each cruise in YV and WV by SCUBA diving by a minimum of two scientific divers. We did not collect organisms outside the YV and WV areas, as they remained mostly unaffected by the vent chemistry in the mixing zone, and the seafloor fauna typically reflect the surrounding shelf benthic habitat (Chan et al., 2016). A total of 12 specimens of *X testudinatus* were collected in 2015, six from YV and six from WV. In 2018, 16 were collected, 10 were collected at the YV and six at the WV. The divers collected crab samples every four meters along a 25 m transect between YV and WV. Key species of gastropods, including sessile (*T. adamsii*) and motile (*B. gravispinosu* and *E. contracta*), were collected in WV within 10 m of the same site each year. At least six specimens of each mollusc species were collected. All organisms were placed in portable nets and brought to the surface where they were placed in aerated containers with seawater. After sampling, the vent invertebrates were transported to the laboratory of the National Taiwan Ocean University and placed in an 80×50×60 cm (L×W×H) tank with constant fresh filtered seawater flow (~25°C, similar to the ambient seawater temperature at KST) for 24 h to empty their gut contents. Unfortunately, numerous samples from the filter feeders *T. adamsii* and *B. gravispinosu* died or were preyed on by carnivorous *E. contracta* or *X. testudinatus* during transport and 24 h of gut cleaning, resulting in final sample sizes of three

per species. The sample size for *E. contracta* was $n = 3$ in 2015 and $n = 6$ in 2018 (Table 1).

In 2015, due to the lack of trained personnel on site to dissect the animals, all vent invertebrates were rinsed in deionized water and then frozen at −20°C before drying in the oven at 60°C for 48 h. The dry samples were then shipped back and dissected at the Kiel University (CAU). In 2018, after being rinsed in deionized water, all molluscan samples were frozen at −20°C for Euthanasia and crabs were desensitized by placing them on ice for half an hour before dissection. The crabs were sexed according to their shape of the pleonal structures during dissection. For crabs, we pooled and analysed claw muscle tissues. For the gastropods, we used all available muscle tissue, including foot and abductor muscles due to the small mass of the specimens. To investigate whether the macrofanua species changed their body sizes in response to biogeochemical changes, we also measured the sizes of *X. testudinatus* and gastropods except for the irregularly coiled *T. adamsii*. We determined the size of *X. testudinatus* by measuring the distance between the two most protruding notches. We used the shell height and length, respectively, to determine the body sizes of the gastropod *E. contracta* and *B. gravispinosu*. All body size data are presented in Supporting Information Table I. Although we used different drying methods, that is, oven drying for samples collected in 2015 and freeze drying for samples collected in 2018, these methods have little effect on the isotope values of benthic macroinvertebrates samples (Akamatsu et al., 2016) (Supporting Information Text III).

To assess the dominant basal resources that fuel the KST food web after the events, we collected seawater POM, chemolithotrophic bacteria (Epsilonproteobacteria) and epilithic green algae (Chlorophyta indet. sp.) in May 2018. We collected vent POM and zooplankton during a subsequent sampling trip in October because the May samples were spoiled after an unexpected electrical outage. Vent POM samples were obtained by filling vent water into 3 L Nalgene bottles in YV ($n = 5$) and WV ($n = 5$). The seawater POM was collected in a similar fashion with three 15 L water jugs, but outside the WV area ($n = 3$). In the mouth of the YV vent, chemolithotrophic bacteria ($n = 2$) were collected by filling several 1 L bottles with plume water near the vent. All of these fluids were kept on ice in the ship and filtered through pre-combusted (500°C) Whiteman GF/C filters immediately after being transported back to the lab. Green algae (Chlorophyta indet. sp.) were collected from the surface of rocks in YV and WV ($n = 5$ in total). Zooplankton were sampled with a handheld plankton net (500 μm mesh) from the three different locations in the peripheral zone outside of YV and WV. For each location, we cast three nets, and waited for at least 15 min before drawing the nets. Then we separated the zooplankton into two fractions by passing the collected sample through a finer mesh size (100 μm). Under the microscope, we further removed fish larvae and jellyfish larvae from zooplankton samples. Food source samples were also freeze-dried for 3 days. At the Institute of Geosciences in CAU, all samples were homogenized using a mortar and pestle and subdivided into two fractions, one for stable C and N isotope analyses and the other for stable S isotope analyses. The isotope data

TABLE 1 Stable isotope values (mean±standard deviation) of the vent crab *X. testudinatus* (pooled from both the YV and WV habitats) and gastropods, as well as potential food sources, in KST in years 2015 and 2018. The individual data for each consumer and food source from this study are presented in Supporting Information Tables S1 and S2.

	Year	Species/sample description	Body width (mm)	$\delta^{13}C$ (‰)	$\delta^{15}N$ (‰)	$\delta^{34}S$ (‰)	Ref. sources
Consumers	2015	*Bostrycapulus gravispinosus* (n = 3)	14.0±0.2	−20.3±0.1	6.7±0.3	9.1±1.1	This study
		Ergalatax contracta (n = 3)	22.3±2.0	−19.7±0.6	8.2±0.4	6.8±0.5	
		Thylacodes adamsii (n = 3)	nd	−21.4±0.3	7.0±0.4	7.2±2.3	
		Xenograpsus testudinatus (n = 12)	21.4±2.8	−15.3±2.1	5.4±0.8	7.8±2.2	
	2018	*Bostrycapulus gravispinosus* (n = 3)	13.2±0.2	−17.5±0.8	2.0±0.7	11.8±0.5	This study
		Ergalatax contracta (n = 6)	20.6±1.6	−15.6±0.4	9.9±0.5	9.9±1.8	
		Thylacodes adamsii (n = 3)	nd	−18.5±0.3	4.1±2.9	12.9±1.6	
		Xenograpsus testudinatus (n = 16)	20.4±3.0	−16.2±1.1	7.5±0.8	5.4±1.5	
Potential food sources	2015	Green turf algae (n = 15)		−22.4±3.1	5.6±1.6	nd	Wang et al. (2022)
		Bacteria from vent water (n = 6)		−21.9±0.9	6.5±3.4	nd	
		Zooplankton (n = 13)		−19.6±1.3	7.2±1.0	nd	
		Vent POM (n = 2)		−18.2±1.1	−1.7±0.4		Chang et al. (2018)
		Seawater POM (n = 17)		−23.4±0.7	5.0±1.1	nd	
	2018	Green algae Chlorophyta indet. sp (n = 5)		−19.6±2.0	5.9±0.9	15.2±3.2	This study
		Bacteria from vent water (n = 2)		−20.1±0.2	5.3±0.1	4.8±1.0	
		Zooplankton (n = 18)		−20.2±0.7	6.8±1.6	17.1±3.1	
		Vent POM (n = 10)		−22.2±0.9	4.2±1.0	4.9±2.7	
		Seawater POM (n = 3)		−20.8±0.2	3.8±1.4	16.0±1.2	

for potential food sources for 2015 were extracted from previously published work (Chang et al., 2018; Wang et al., 2022).

2.2 | Stable carbon and nitrogen isotope analyses

For samples collected in 2015, approximately 60–100 μg of dry mass for each sample was analysed for stable C and N isotope ratios using a continuous flow isotope ratio mass spectrometer MAT253 (Thermo Finnigan) coupled to an elemental analyser EA1108 (Carlo Erba Instruments) (EA-IRMS) through a Conflo III interface (ThermoFinnigan) in the stable isotope facility of the University of La Coruña, Spain. The isotope data are expressed in delta (δ) permil (‰): $\delta(‰) = [(R_{sample}/R_{standard}) - 1] \times 1000$, where R is the ratio of heavy to light isotope. The isotope ratios are expressed relative to international standards: VPDB for carbon and atmospheric air for nitrogen. During the analyses, a set of international reference materials was used for measurement calibration (NBS 22, IAEA-CH-6, USGS24 for δ^{13}C and IAEA-N-1, IAEA-N-2, IAEA-NO-3 for δ^{15}N). Analytical measurement errors of ±0.15 ‰ were calculated for δ^{13}C and δ^{15}N based on the replicated analyses of laboratory standard acetanilide interspersed between sample analyses. Samples collected in 2018 were measured with an EA-IRMS in the Iso Analytical Limited Inc, UK. Approximately 1 mg of the dry mass of each sample was used for the carbon and nitrogen isotope analysis. For quality control, internal lab standards (IA-R068, IA-R038, IA-R069, and a mixture of IAEA-C7 and IA-R-R046) were analysed between sample runs. These standards were calibrated against the international reference material IAEA-CH-6, IAEA-N-1, IAEA-C-7 for both δ^{13}C and δ^{15}N. The internal standards measured for bulk δ^{13}C and δ^{15}N analyses during the sample sequence yielded 1σ = 0.03‰ and 0.03‰, respectively. About 20% of our samples were performed in duplicate in each laboratory to ensure the reproductivity of the measurement. These duplicate samples are identical to or within the reported analytical uncertainties. For organisms with C:N > 3.5, we applied lipid correction to δ^{13}C values for muscle tissue samples (n = 49) following Logan et al. (2008). We did not perform lipid extraction prior to stable isotope analyses of muscle tissues because lipid extraction is known to affect δ^{15}N values (Svensson et al., 2016).

2.3 | Stable sulphur isotope analyses

Sulphur isotope analyses were performed on an EA-IRMS at Iso-Analytical Limited, UK. Tin capsules containing reference or sample material plus vanadium pentoxide catalyst were loaded into an automatic sampler, dropped, in sequence, into a furnace held at 1080°C, and combusted with oxygen. For quality control purposes, test samples of a set of internal standards IA-R061 (barium sulphate) (n = 12), IAEA-SO-5 (barium sulphate) (n = 5), IA-R068 (soy protein) (n = 5), and IA-R069 (tuna protein) (n = 3) were measured during batch analysis of our samples. Internal laboratory standards, IA-R061, IA-R025 (barium sulphate), and IA-R026 (silver sulphide), were used to calibrate and correct for ^{18}O contribution to the SO$^+$ ion beam. The

calibration of internal standards was performed against interlaboratory comparison standards (NBS-127, barium sulphate and IAEA-S-1, silver sulphide) distributed by the International Atomic Energy Agency. The standard deviation for the test samples was ±0.10‰ except for IA-R069 (±0.32‰). The sulphur isotope ratios are also expressed in delta (δ) permil (‰) relative to the international standard Vienna Canyon Diablo Troilite (V-CTD); 20% of the samples were run in duplicate to ensure the reproductivity of the measurement. The results of these duplicate samples yield identical results or within the analytical uncertainties.

2.4 | Change in *X. testudinatus* population density from 2004 to 2018

To understand whether decreased vent activity at the KST affected the population of *X. testudinatus*, we investigated the correlation between vent activity and crab abundance by conducting an underwater video survey near the new YV mouths (121.962°E, 24.834°N, Supporting Information Figure I), the most populous area for *X. testudinatus*. A digital camera was set up to capture the $50 \times 88 \, cm^2$ area for 3 days from 10 August to 12 August 2018. To be consistent with previous published population data, which were only captured during the day, we used footage from only daylight hours for population density analysis, and images were analysed when image quality was adequate. To count the mobile specimens that entered the survey area, we divided each hour into six 10-min intervals, which amounted to 66 film frames that were used for this analysis. The estimated density from this footage is 26 ± 9 specimens at $50 \times 88 \, cm^2$. We then compared our counts with the baseline population of *X. testudinatus* established in 2004 and 2014 (Chan et al., 2016; Jeng et al., 2004). To make the density data comparable on all sampling occasions, we standardized the density of *X. testudinatus* to individuals per m^2 (Table 2). All three studies used different methods to estimate densities. Jeng et al. (2004) remarked that their method of collecting samples from an area of $0.25 \, m^2$ with a net most likely underestimated the density because there was a higher density of crabs hiding in the rocky crevasse. Chan et al. (2016) surveyed from a broader area at KST. They placed three quadrats ($25 \times 25 \, cm$) every 5 m along a 50 m transect at 10 different stations in 2014. The number of mobile individuals was counted inside the quadrat according to the photograph; however, these authors also noted that their

TABLE 2 Vent crab population density data at the YV from 2004 to 2018.

Year	Average density ($1 \times 1 \, m^2$)	SD	Reference
2004	364	Not reported	Jeng et al. (2004)
2014	176	96	Chan et al. (2016)
2018	59	20	This study

approach may underestimate the population density because some specimens moved when the quadrats were placed.

2.5 | Statistical analyses

All statistical analyses were performed in R version 4.1.0 (R Core Team, 2020) using the R-Studio interface. Isotope data (δ^{13}C, δ^{15}N, and δ^{34}S) of all consumers were assessed for homoscedasticity using Fligner-Killeen tests and visualized for any deviations from normality in the QQ plot. We found *P values* of 0.87 (Chi-squared = 0.71, *df* = 3), 0.24 (Chi-squared = 4.2, *df* = 3), and 0.29 (Chi-squared = 3.8, *df*-3) for δ^{13}C, δ^{15}N, and δ^{34}S respectively. Given that all *p*-values are >0.05, this indicates that the isotopic variance in all organisms was homogeneous. All of the isotope values were also evaluated (R function: cor) for their correlation with each other, and we found that none of the parameters correlated with one another. On the basis of these tests, we carried out statistical analyses on the isotope results. We first tested for significant changes of δ^{13}C and δ^{15}N in vent POM and seawater POM from 2015 and 2018 using two sample *t*-tests. To determine if there were any differences in the isotope values of *X. testudinatus* based on habitat (i.e., YV vs. WV) and sex (female vs. male), multivariate analysis of variance (MANOVA) and univariate analysis of variance (ANOVA) tests were conducted for 2018 samples. The sample sizes for YV and WV were 6 and 10, respectively, while the sample size for each sex was 8. No significant differences were found between habitats and sex, so all *X. testudinatus* were combined for subsequent analyses. We conducted a MANOVA Pillai's trace test to determine significant changes in the inter-annual isotope values (δ^{13}C, δ^{15}N, and δ^{34}S) between *X. testudinatus* collections from 2015 and 2018. The MANOVA test was used for comparison for *X. testudinatus* in 2015 and 2018 as its assumptions were satisfied. To identify which dependent variables (δ^{13}C, δ^{34}S and/or δ^{15}N values) were significantly different between 2 years, ANOVA was performed on the MANOVA output (R function: summary.aov). For the mollusc species, we performed a two-sample t-test on the isotopic changes on *E. contracta* before and after the extreme events. The test was performed as both the standard population effect size (*D* > 4) and sample sizes met the statistical assumption (De Winter, 2013). However, no statistical analyses were performed on *B. gravispinosus* and *T. adamsii* due to small sample sizes (*n* = 3; De Winter, 2013). We tested for significant differences in the intra-annual variability of isotope values (δ^{13}C, δ^{15}N, and δ^{34}S) between *X. testudinatus* and the pooled gastropod species by performing MANOVA and ANOVA analyses. We compared all three isotope variables (δ^{13}C, δ^{15}N, and δ^{34}S) for 2015 but only δ^{13}C and δ^{34}S for 2018, as the full δ^{15}N value ranges of gastropods were wider in comparison to those of *X. testudinatus* in 2018. Additionally, a two-sample *t*-test was used to examine changes in body size between 2015 and 2018 (before and after the extreme events). The *p*-adjusted values from all ANOVA decomposition tests were obtained using the *p.adjust* function with the FDR method. Unless otherwise stated, statistical significance is assessed at *p* <0.01. Finally, we calculated the standard ellipse area (SEA) of

the bivariate isotope space for each consumer group, also known as the isotopic niche space, at a 95% confidence interval using R package SIBER (Jackson et al., 2011). Because the calculation of the niche space requires a minimum of five data points for each group to calculate the covariance matrix (Jackson et al., 2011), we only report but do not discuss the isotopic niche space for filter feeding molluscs due to their small sample sizes (*n* = 3). Likewise, we did not use a Bayesian mixing model to calculate the proportional contributions of potential food sources because our mixing space is incomplete, that is, the isotopic values of some potential sources are not known (Supporting Information Discussion I). Missing dietary sources will result in inaccurate estimation of proportional contribution (Weltje, 1997). All figures are made using "ggplot2" (Wickham, 2016).

2.6 | Stable isotope compilation of deep-sea benthic fauna

To put the KST faunal dataset in a global context, we collected the δ^{34}S, δ^{13}C, and δ^{15}N values from DeepIso database (https://www.se-anoe.org/data/00654/76595/; Michel et al., 2021) and several other studies (Erickson et al., 2009; Fry et al., 1983). DeepIso is a publicly assessable database of stable isotope ratios and elemental contents for deep-sea ecosystems. We primarily gathered faunal data from various deep-sea hydrothermal vents in the Pacific Ocean including active and inactive vents, cold seeps, as well as non-vent deep-sea benthic fauna. We only selected soft tissue data obtained from samples that were preserved in conditions similar to our own samples, either dry or frozen.

3 | RESULTS

3.1 | Isotope changes of potential sources from 2015 to 2018

The mean and standard deviation of the isotope values of consumers and potential food sources are presented in Table 1. Individual data are presented in Supporting Information Table S2. The food isotope values include published data from 2015 (Chang et al., 2018; Wang et al., 2022) and our own data from 2018. In terms of δ^{15}N, seawater POM, green algae, bacteria, and zooplankton ranged between 5.0 and 7.2‰ in 2015, which was significantly higher than that of vent POM at −1.7‰. In 2018, average seawater POM decreased to 3.8‰, but the change was not significant from that in 2015 (t_{10} = 1.85, *p*-adj = 0.09). On the contrary, the vent POM increased to 4.2‰ and was significantly higher than that of 2015 (t_{11} = -7.8, *p*-adj < 0.0001). In terms of δ^{13}C, non-POM resources ranged between −22.4 and −19.6‰ in both years. From 2015 to 2018, seawater POM changed from −23.4 to −20.8‰ (t_{10} = −10.9, *p*-adj <0.0001), and the vent POM from −18.2‰ to −22.2‰ (t_{11} = 5.7, *p*-adj = 0.00014). In terms of δ^{34}S, values of bacterial POM (4.8‰) and vent POM (4.9‰) in 2018 were much closer to the KST native sulphur (1.1‰) than to

seawater POM (16.0‰), which is closer to the KST seawater sulphate (20.6‰) (Chen et al., 2005).

3.2 | δ^{34}S, δ^{13}C, and δ^{15}N of *X. testudinatus* by habitat and sex in 2018

We did not detect significant isotopic differences between *X. testudinatus* collected in YV and WV in 2018 (MANOVA Pillai's trace = 0.49, $F_{3,12}$ = 3.80; *p*-adj = 0.08, Supporting Information Table S3). The values of δ^{34}S, δ^{13}C and δ^{15}N at both sites were identical (ANOVA *p*-adj = 0.41, 0.03, and 0.16, respectively). Therefore, the isotope data from these two sites were pooled for *X. testudinatus* for further analyses. Despite some of the *X. testudinatus* females carrying eggs at the time of sampling, there were no differences in isotope values between the sexes (female vs. male) in 2018 (Pillai's trace = 0.27, $F_{3,12}$ = 1.49; *p*-adj = 0.27, Supporting Information Table S4). Therefore, the isotope data for the two sexes were also pooled in the following results.

3.3 | Interannual variability in δ^{34}S, δ^{13}C, and δ^{15}N of *X. testudinatus* between 2015 and 2018

The isotope values for *X. testudinatus* between 2015 and 2018 were significantly different (Table 1, MANOVA Pillai's trace = 0.8, $F_{3,24}$ = 34.9; *p* < 0.0001). These differences were mainly driven by changes in δ^{34}S and δ^{15}N (ANOVA, *p*-adj = 0.003 and *p*-adj < 0.0001 for δ^{34}S and δ^{15}N, respectively; Supporting Information Table S5). Interestingly, the direction of change for δ^{34}S and δ^{15}N also differed. For example, the average δ^{34}S values decreased ~2.4‰, whereas the δ^{15}N values increased ~2.1‰ from 2015 to 2018. In contrast, the δ^{13}C values between these 2 years were not statistically different (ANOVA, *p*-adj = 0.18, Supporting Information Table S5), and the mean δ^{13}C values were −15.3 ± 2.1‰ for 2015 and −16.2 ± 1.1‰ for 2018 (Table 1).

3.4 | Interannual variability in δ^{34}S, δ^{13}C, and δ^{15}N of gastropods between 2015 and 2018

The shifts in δ^{34}S, δ^{13}C, and δ^{15}N values for suspension feeding gastropods before and after the extreme events were noticeable (Figure 3). Unfortunately, the low number of replicates for these suspension feeders did not allow us to perform species-specific statistical analyses (Supporting Information Figure S2). On average, δ^{34}S values increased after the event by ~3‰ for *B. gravispinosus* and ~5‰ for *T. adamsii*, and δ^{13}C values increased by ~3‰ for both species. The temporal differences were greater than the intraspecies variability (Table 1). In contrast, δ^{15}N values of these two suspension feeders decreased by ~5‰ for *B. gravispinosus* and ~3‰ for *T. adamsii*. Their intraspecific variabilities increased substantially after these extreme events. For the carnivorous mollusc *E. contracta*, all isotope values increased significantly after extreme events (two sample *t*-tests: t_5 = 3.7, *p*-adj = 0.01; t_7 = 12.6 and *p*-adj < 0.0001; t_7 = 5.0 and *p*-adj = 0.002 for δ^{34}S, δ^{13}C, and δ^{15}N respectively; Supporting Information Table S6).

3.5 | Intra-annual variability in δ^{34}S, δ^{13}C, and δ^{15}N between *X. testudinatus* and gastropods

X. testudinatus and the gastropods occupied different isotopic niche spaces. Their differences were driven by a different isotope each year (Figure 3). The significant difference between the endemic *X. testudinatus* and the non-endemic gastropods in 2015 (Pillai's trace = 0.8, $F_{3,17}$ = 22.6; *p*-adj < 0.0001) was driven by differences in δ^{13}C and δ^{15}N values (ANOVA, *p*-adj < 0.0001, Supporting Information Table S7), but not δ^{34}S (ANOVA, *p*-adj = 0.9). In 2018, the significant differences (MANOVA Pillai's Trace = 0.77, $F_{2,24}$ = 40.1; *p*-adj < 0.0001, Supporting Information Table S8) were driven by δ^{34}S (ANOVA *p*-adj < 0.0001, Supporting Information Table S8) rather than δ^{13}C changes (ANOVA *p*-adj = 0.19). The average δ^{13}C values were almost identical (−16.2‰ and −16.8‰ for *X. testudinatus* and gastropods, respectively).

3.6 | Population size and body sizes and changes before and after the extreme events

The average population of *X. testudinatus* gradually declined from 2004 to 2016, but the rate of this decline doubled after the extreme events in 2016. In 2004, the average density count was 364 per m^2 at the YV (Jeng et al., 2004). By 2014, the density was down to 176 ± 96 per m^2 at the YV (Chan et al., 2016). Assuming that the decline rate is linear, this equates to a decline rate of ~19 per m^2 per year from 2004 to 2014 (a 10-year period). In 2018, the density of *X. testudinatus* dropped to 59 ± 20 per m^2 (Table 2), which equates to a decline rate of 40 individuals per m^2 per year from 2016 to 2018 (two-year period). We did not observe any apparent changes in the density of the gastropod population after the earthquake. Two sample t-tests on body width of *X. testudinatus* and *E. contracta* showed that their body size did not change significantly after disturbances (t_{26} = −0.94, *p*-adj = 0.35 for crabs; and t_7 = −0.141, *p*-adj = 0.20 for *E. contracta*, respectively). The body size of *B. gravispinosus* is similar to the previous observation (Chen et al., 2017) and did not change significantly before and after the extreme events (t_4 = −0.41, *p*-adj = 0.05).

3.7 | δ^{34}S, δ^{13}C, and δ^{15}N niche space changes before and after extreme events

The δ^{34}S, δ^{13}C and δ^{15}N niche space for *X. testudinatus* became narrower after disturbance (Supporting Information Table S9). The corrected Standard Ellipse Area (SEAc, ‰^{2}) of the δ^{13}C and δ^{15}N niche

FIGURE 3 Stable isotope biplots of endemic vent crabs (*Xenograpsus testudinatus*) and non-endemic gastropods: a sessile suspension feeder limpet (*Bostrycapulus gravispinosus*), a mobile suspension feeder snail (*Thylacodes adamsii*), and carnivorous scavenger snail (*Ergalatax contracta*) from the KST in years 2015 (before an earthquake and typhoon) and 2018 (after an earthquake and a typhoon): (a) δ^{13}C and δ^{15}N; (b) δ^{34}S and δ^{13}C. The average isotope values of the potential food source, such as zooplanktoon (black open square), green algae (black open circle), and bacteria (gray open diamond), seawater POM (light blue dash triangle), vent POM (orange triangle) from previous work (Chang et al., 2018; Wang et al., 2022) and this work are also plotted. Additionally, we also plotted seawater sulphate (light blue dash lines) and δ^{34}S value of native sulphur (orange dash lines) ($n = 5$; Chen et al., 2005).
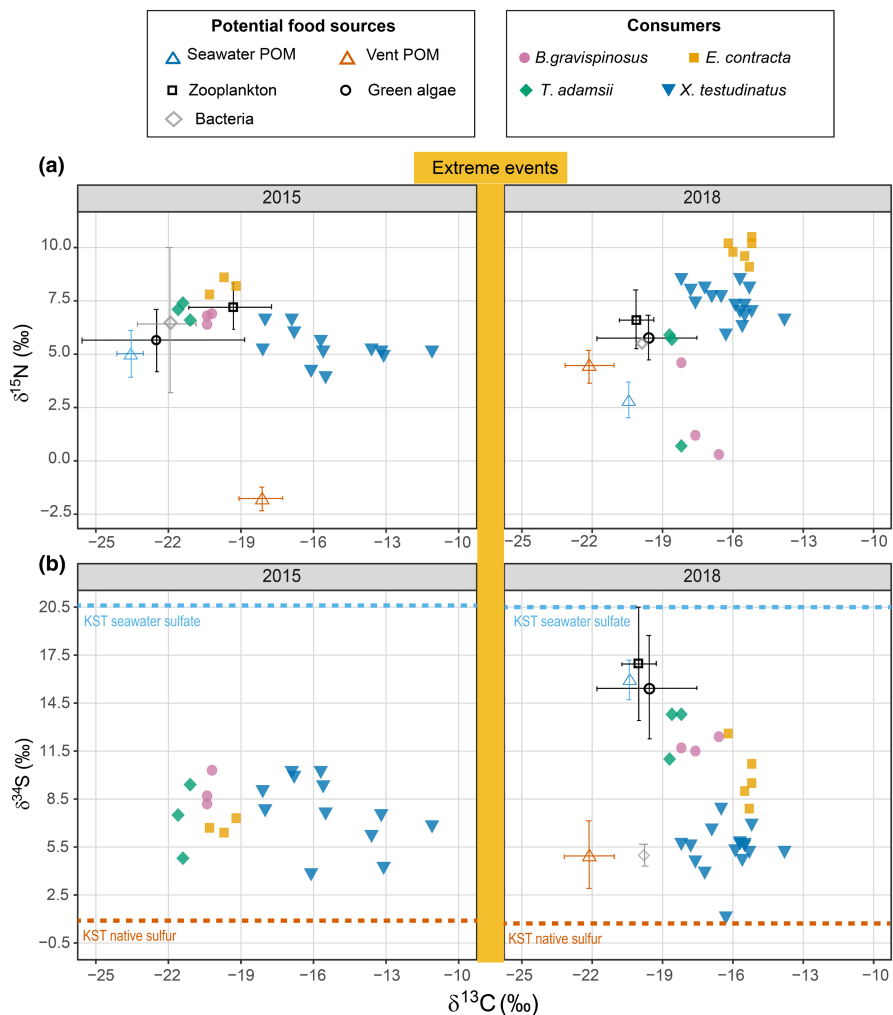
space changed from 5.6 to 2.6 and the SEAc of the δ^{34}S and δ^{13}C space decreased from 14.3 to 5.6. For the carnivorous mollusc *E. contracta*, the δ^{13}C and δ^{15}N niche space became narrower with SEAc shifting from 1.2 to 0.9, whereas the δ^{34}S and δ^{13}C niche space became wider with SEAc shifting from 1.3 to 2.2 due to the broadening the δ^{34}S space.

4 | DISCUSSION

4.1 | Extreme events triggered drastic changes in sulphur cycling

The extreme events caused a major change in sulphur cycling. Native sulphur balls and chimneys completely disappeared at KST. Before the extreme events, sulphur dioxide (SO_2) predominated over hydrogen sulphide (H_2S) in the vent fluids at KST, leading to precipitation and formation of bright yellow native sulphur chimneys and balls. The following chemical reactions between the different sulphur species have been proposed to explain the occurrence of sulphate and the accumulation of native sulphur in acidic hydrothermal and volcanic conditions (Iwaji & Takejiro, 1960; Oana & Ishikawa, 1966):

$$SO_2 + H_2O \rightarrow H_2SO_3, \quad (1)$$

$$3H_2SO_3 = 2H_2SO_4 + S + H_2O. \quad (2)$$
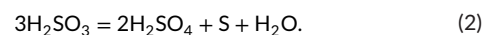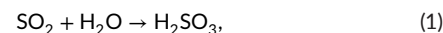
As long as there is sulphurous acid in the solution (Equation 2), this reaction is maintained to produce native sulphur. However, as soon as the sulphurous acid disappears, the native sulphur starts to decrease and eventually disappears because S reacts with water to produce H_2S and H_2SO_4:

$$8S + 8H_2O \rightarrow 6H_2S + 2H_2SO_4. \quad (3)$$
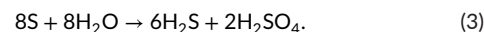
This phenomenon has been observed in other hydrothermal and volcanic settings (Oana & Ishikawa, 1966). Therefore, we posit that the disappearance of previously abundant native yellow sulphur accretions on the seafloor near the active YV (Figures 1 and 2) after the earthquake and typhoon is due to vent fluid shifting from an oxidizing to a reductive state (a decreasing ratio of SO_2 to H_2S), which lowered SO_2 and, ultimately, H_2SO_3 concentrations (de Ronde et al., 2001). A sulphur reductive state also resulted in a more pronounced ^{34}S depletion of sulphides and other sulphur species in the

vent fluids (Sakai, 1968; Ueda et al., 1979). In addition to changes in sulphur speciation, there was also a significant reduction in sulphur fluid fluxes from the YV after the extreme disturbance, leading to an increased influence of seawater sulphate (more ^{34}S depleted) in the mixing zone. Taken together, these processes played an important role in the sulphur availability of chemosynthetic organisms (e.g., chemotrophic bacteria, vent POM, etc.) versus photosynthetic organisms (e.g., seawater POM, phytoplankton, etc.) at the base of the food web (Figure 2a,b).

The δ^{34}S values of *X. testudinatus* and gastropods were identical before the extreme events when the venting activities were strong (Figure 3b). This indicates that before the disturbance, the YV fluids were the dominant source of sulphur for primary production in the KST area, effectively obscuring any potential effects of the sulphur source in seawater (Chen et al., 2005) (Figure 2a). This is due to the high S^{2-} concentration in the YV fluids, which was approximately five times higher than that of the WV fluids and fifty times that of seawater in the Kuroshio Current (Chen et al., 2005; Wu et al., 2014). After the extreme events, the reduced sulphur flux from the vent decreased their dominance as the main source of sulphur in the KST region. This resulted in a shift towards an increased reliance on photosynthetic primary production closer to vents. This change indicates that the vent sulphur is no longer the dominant sulphur source for the entire KST, making ^{34}S an informative tracer to distinguish between chemo- and photosynthetic origins (Figure 2b).

4.2 | Controls on δ^{13}C and δ^{15}N values of dietary sources

Stable carbon isotope ratios are the optimal tracer for assessing the dietary contribution to the vent animals prior to the extreme events. We suggest that the δ^{13}C values at KST were controlled by the mode of carbon fixation rather than the source of carbon. The primary pathways for carbon fixation are likely to be through (1) Calvin cycle photosynthesis or (2) the reductive tricarboxylic acid cycle utilized by certain sulphur chemoautotrophs (Hügler & Sievert, 2011; Wang et al., 2018). The Calvin cycle results leads to lower δ^{13}C values, while the reductive tricarboxylic acid cycle leads to higher δ^{13}C values. These fractionations were evident in the distinct δ^{13}C differences between the two main sources of POM, seawater (−23‰) and vent (−17‰) POM prior to the extreme events in the KST region (Chang et al., 2018). The data in Figure 3 also support the conclusion that the contribution of methanotrophic production to the KST food web was minimal. This is due to the fact that the seawater POM in 2015 had the most negative δ^{13}C values among all basal resources and consumers, while methanotrophic production typically yielded δ^{13}C values below −35‰ (Wang et al., 2022). Regarding nitrogen, the potential controls of vent derived δ^{15}N values are not well understood (see Section 1). However, the fact that the values of vent POM became more ^{15}N enriched and converged upon those of seawater POM after the

disturbance while seawater POM became more ^{15}N depleted suggests that a higher contribution of nitrogen-fixing cyanobacterial production to the KST system may have played a role.

4.3 | Dietary response to the drastic biogeochemical changes and habitat disruption

According to the stable sulphur, carbon, and nitrogen isotope framework presented above, this study suggests a strong nutritional link between the model species *X. testudinatus* and chemoautotrophic sources. This is shown by the higher δ^{13}C values of *X. testudinatus* (−15.3±2.1‰; 2015) compared to gastropods (average −20.5±0.7‰; 2015; Figure 3a). These results concur with previous studies at KST (Chang et al., 2018; Wang et al., 2014). However, the δ^{13}C values of *X. testudinatus* were higher than any of the sampled food sources, including macroalgae and vent POM (ranging from −27 to −17‰). This suggests that we were unable to sample an important dietary component, such as ^{13}C-enriched chemosynthetic bacteria that use the reductive tricarboxylic acid carbon fixation. Therefore, we could not estimate different source contributions to consumers using a Bayesian mixing model approach (Supporting Information Discussion I). The absence of the source does not change our conclusion because the δ^{34}S values after the disturbance provide clear evidence that chemosynthetic bacteria make important nutritional contribution to *X. testudinatus*. Firstly, the δ^{34}S values of *X. testudinatus* are more similar to those of vent POM and bacteria than to those of non-vent sources including macroalgae, zooplankton, and seawater POM (Figure 3). Secondly, despite a decrease in chemosynthetic primary production along the transect from the YV to the WV peripheral area (Figure 2), the δ^{34}S values of *X. testudinatus* decreased by 2.5‰, indicating continued nutrient intake from vent sources (Figure 3). Thirdly, the δ^{34}S values of *X. testudinatus* were similar in the WV and YV habitats, reinforcing the idea that *X. testudinatus* has an obligate nutritional relationship with vent production, despite its ability to supplement with non-vent resources.

The decrease in δ^{34}S values in *X. testudinatus* is likely due to depletion in ^{34}S in vent sourced diet, triggered by sulphur speciation (Figure 2). The shift from a more oxidizing to a reductive state led to the disappearance of native sulphur at KST, causing a more pronounced ^{34}S depletion of sulphides and the overall sulphur species in the vent fluids (Sakai, 1968; Ueda et al., 1979). It is unlikely that POM decomposition in the sediment contributed to the production of sulphide, as KST is a shallow system with limited deposition of organic matter. Additionally, the decrease in δ^{34}S values was not due to an increase or preferential intake of chemosynthetic sources by *X. testudinatus*. This is because when the KST vent activities decreased after the extreme disturbance, fewer sulphur chemotrophic bacteria became available as a food source. For example, a noticeable reduction in the intensity of the conspicuous white colour produced by the dominant chemoautotrophic sulphur bacteria, such as epsilonproteobacteria and gammaproteobacteria, was observed in WV seawater after the extreme events (Lebrato et al., 2019, Supporting Information Video S3).

We found that gastropods in the WV consistently relied more on photosynthetic sources than on chemosynthetic sources. Before the extreme events, the gastropods had more negative $\delta^{13}C$ values (~21‰) than those of the crabs (~15‰). Given that seawater POM was −23.4‰ and vent fluid POM was −18.2‰ in 2015 (Chang et al., 2018), our study confirms previously published data that the gastropods relied less on chemosynthetic

sources than *X. testudinatus* (Chang et al., 2018; Wang et al., 2014). After the events, the marked increased $\delta^{34}S$ values in gastropods suggest that gastropods relied more on photosynthetic sources and became closer to benthic organisms in the open ocean (ranging from +6 to +23‰ with an average of 16.1‰, Figure 4a), reflecting the increased dominance of the photosynthetic energy channel.
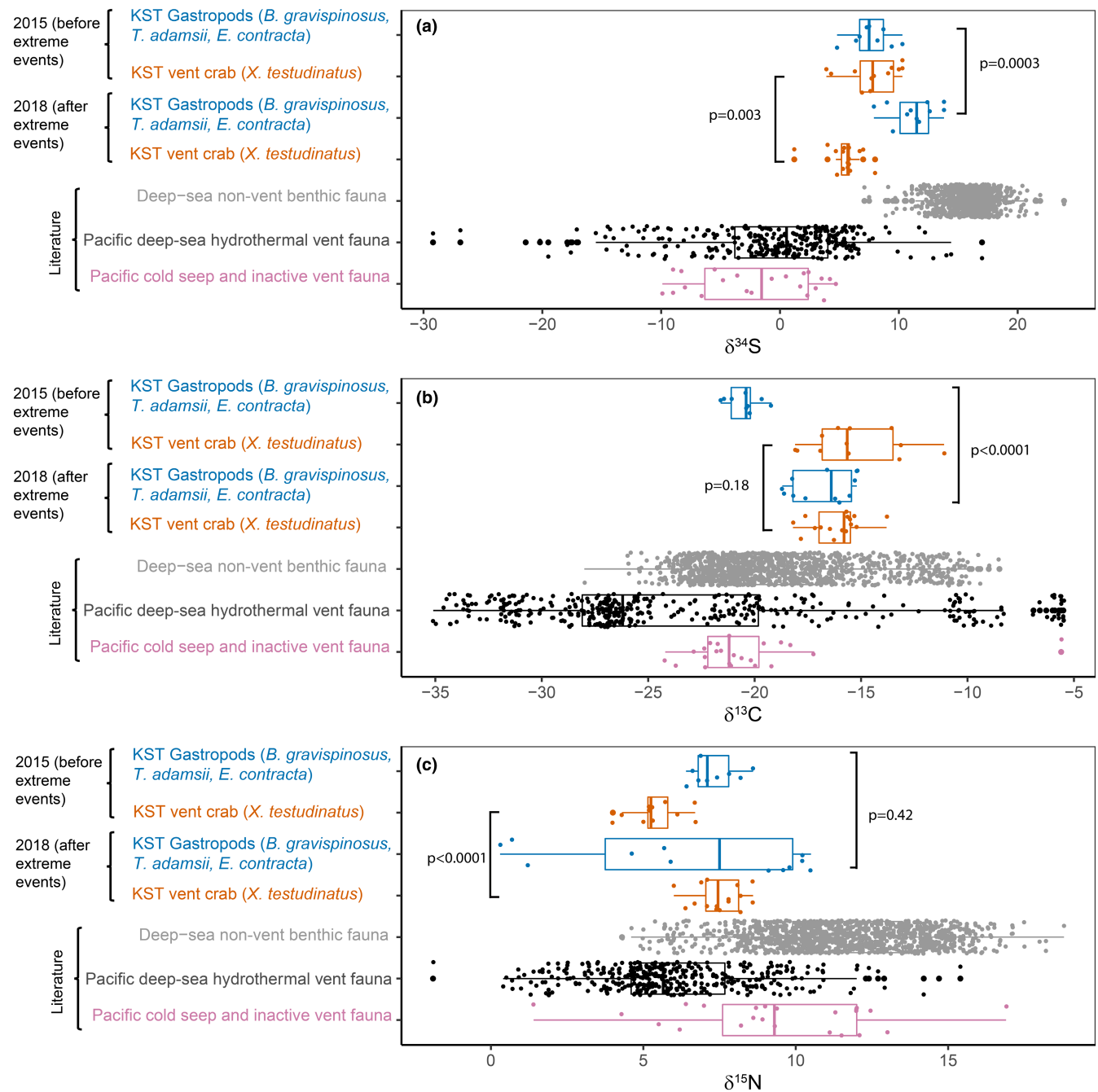

FIGURE 4 $\delta^{34}S$, $\delta^{13}C$, and $\delta^{15}N$ values of KST fauna before and after the extreme events compared to the literature isotope values of the benthic fauna from the hydrothermal vent, cold seep, and inactive vent in the Pacific Ocean and deep-sea benthic fauna in the open ocean. Most of the literature data were extracted from Database DeepIso—a global open database of stable isotope ratios and elemental contents for deep-sea ecosystems (https://www.seanoe.org/data/00654/76595/; Michel et al., 2021). However, we did not include any isotope data analysed from samples that have been preserved in ethanol or formaldehyde in this dataset. Additional data from Pacific are also included (Erickson et al., 2009; Fry et al., 1983). These global reference data are individual data points or composite tissue data.

The disturbance in KST caused a marked shift in the δ^{15}N values among gastropods and *X. testudinatus* (Figure 3, Table S4). The δ^{15}N values of *X. testudinatus* and carnivorous *E. contracta* increased by 2‰, concomitant with an increase in vent POM by 5‰, suggesting that the δ^{15}N increase of the two species was associated with changes in the vent sources rather than trophic position. The δ^{15}N values of zooplankton remain unchanged, most likely dissociated with vent changes because their δ^{34}S values indicate a seawater-dominated energy channel for both years. The suspension feeders showed a more diverse response, with half having δ^{15}N values around 5‰ and the other half approaching 0‰. All suspension feeders had seawater-like δ^{34}S values after the disturbance at the KST. Taken together, we posit that two groups of suspension feeders (with different δ^{15}N values) were fuelled by two different phytoplankton energy channels: diazotrophic cyanobacteria versus non-diazotrophic cyanobacteria and/or eukaryotic phytoplankton. Low δ^{15}N values are characteristic of biomass produced through dinitrogen fixation (Carpenter et al., 1997; Minagawa & Wada, 1986). The KST area in the East China Sea is known to have a high abundance of diazotrophic *Trichodesmium*, which had δ^{15}N values ranging from −2 to +1‰ (Minagawa & Wada, 1986; Wada & Hattori, 1976). The presence of *trichodesmium* at our sites is probably influenced by the flow of the Kuroshio Current through the KST area (Shiozaki et al., 2015; Wu et al., 2018). Before the extreme events, high concentrations of toxic metals such as arsenic, cadmium, copper, and lead could have suppressed cyanobacterial production (Yadav et al., 2016). However, the sharp decrease in toxic metals after the events (Lebrato et al., 2019) could have led to a surge in cyanobacterial production in the KST vent area. Future isotope research should aim to sample and analyse potential dietary sources, including diazotrophic and non-diazotrophic cyanobacteria in the KST region, to make a robust source inference (Supporting Information Discussion I).

4.4 | Dietary changes and foraging adaptations of endemic species

The extreme disturbances at KST provided a unique opportunity to study the response of the endemic species *X. testudinatus* to drastic reductions in vent activities and changes in sulphur cycling. *X. testudinatus* is found only in shallow hydrothermal vents with high sulphur concentrations and has only been spotted in three such locations (Allen et al., 2020; Ho et al., 2015; Hu et al., 2012; Miyake et al., 2019). Despite the greatly reduced chemosynthetic production after the YV became less active, *X. testudinatus* continued to partially rely on chemosynthetic resources, indicating an obligate nutritional relationship with chemosynthetic bacteria (Chang et al., 2018). The drastic population decline and reduced isotopic niche space of *X. testudinatus* after the disturbance further support its status as an obligate feeder of sulphur-dependent bacteria. The reduced niche space is likely due to the decreased influence of vent sulphur that lowered the overall production of

chemosynthetic bacteria. The decline in population is unlikely to have been caused by increased predation, as the vent area remained toxic and off-limits to big predators even after the disturbance occurred.

In terms of fitness effects, a lingering question is whether the alleged nutritional dependence on chemosynthetic production affects the survival of *X. testudinatus* specimens or the reproductive success of the species. *X. testudinatus* has been observed to survive prolonged food scarcity by storing nutrients and supplementing its nutrition via ingestion of non-sulphur bacterial derived resources (Hu et al., 2012). This observation supports that the rapid decline in population after 2016 is linked to decreased fitness as a result of lower chemosynthetic production. It is still unclear how *X. testudinatus* forms its nutritional dependence with sulphur-dependent bacteria, via direct feeding or via direct nutritional transfer from symbiotrophic chemosynthetic bacteria to host (Ponsard et al., 2013; Yang et al., 2016). Regardless of how *X. testudinatus* forms its nutritional dependence with sulphur-dependent bacteria, the sparse geographical distribution of *X. testudinatus* and their rapid population decline after the decreased YV activities show that it is much more vulnerable to vent shutdown than the non-endemic gastropods. In deep-sea hydrothermal ecosystems, many endemic species, such as shrimps, vestimentiferan tube worms, bivalves, and gastropods, also form close associations with sulphur-dependent bacteria (Figure 4). Since these specializations are the result of adapting to an extreme and variable biogeochemical environment over geological timescales, we suggest that endemic vent species, in general, are vulnerable to drastic and sustained disturbances.

4.5 | Dietary changes and foraging adaptations of non-endemic species

These non-endemic gastropods can inhabit different environments and are widely distributed in different world oceans (i.e., Indian or Pacific Oceans). Our study shows that the food sources in KST were strongly affected by the biogeochemical disruption, but the gastropods were less constrained than *X. testudinatus* in their ability to exploit different chemo- and photosynthetic sources. After the disruption, the suspension feeders were able to rely on new dietary sources, including cyanobacteria, and the carnivorous gastropods appeared to increase their δ^{34}S niche space, presumably by foraging closer to the YV area. Furthermore, the abundances and body sizes of the gastropods remain unchanged after the disturbance (Chan et al., 2016 and Supporting Information Table S1), further suggesting their ability to adapt to changing environmental conditions. Together with their tolerance to low- and medium-toxic environments, their flexible dietary niche probably plays an important role in their ability to colonize the transitional environment between the extreme hydrothermal vent and the open pelagic habitat.

4.6 | Foraging adaptations in a dynamic system with frequent disturbances

Our study that covered a major natural disturbance illustrates the consequences of extreme perturbations and makes two important advances. First, we demonstrate that extreme events can dramatically alter the biogeochemical cycling of shallow marine hydrothermal ecosystems, affecting food sources from photosynthetic and chemosynthetic origins. Second, our results show species-specific responses to extreme events in different habitats. These findings are important for assessing the ecological ramifications of human activities, such as changing biogeochemical cycles, unrestrained human development, deep-sea mining, and industrial dredging (Levin et al., 2016; Ramirez-Llodra et al., 2011; Suzuki et al., 2018). After such alterations, benthic habitat may pass a threshold after which they become uninhabitable for endemic species (Cigliano et al., 2010; Hall–Spencer et al., 2002), making marine specialists more vulnerable to the unprecedented evolutionary pressure from human activities than generalist species. On the contrary, generalist species with broad dietary niches and tolerance to rapid changes in biogeochemistry will become more competitive under frequent and severe disturbances from natural hazards and human activities. This study underscores the need for more work on other spatially fragmented habitats containing macrofaunal assemblages comprising rare, endangered, or endemic species. As perturbations become more frequent and intense, more marine habitats will be affected, making long-term monitoring of these habitats important for tracking ecosystem health.

AUTHOR CONTRIBUTIONS

Yiming V. Wang, Mario Lebrato, Dieter Garbe-Schönberg, Li-Chun Tseng and Jiang-Shiou Hwang designed the work. Yiming V. Wang, Mario Lebrato, Li-Chun Tseng, Pei-Wen Lee and Nicolás Sánchez conducted the field work and collected samples. Yiming V. Wang, Nicolás Sánchez and Pei-Wen Lee conducted the lab work. Yiming V. Wang and Thomas Larsen analysed the isotope data. Tin-Yam Chan provided the underwater digital film recording in 2018; Pei-Wen Lee analysed the film data and calculated the vent crab numbers. Yiming V. Wang and Thomas Larsen wrote the manuscript. All authors commented on the manuscripts. Cruises were coordinated by: Mario Lebrato, Dieter Garbe-Schönberg, Li-Chun Tseng and Jiang-Shiou Hwang.

DATA AVAILABILITY STATEMENT

Data are available from the Zenodo online Repository: https://doi.org/10.5281/zenodo.7680525 (Wang et al., 2023). The Arial photo images associated with this study can be found in the Supplementary Video S1, S2, and S3.

ORCID

Yiming V. Wang 🅭 https://orcid.org/0000-0003-3228-5592
Thomas Larsen 🅭 https://orcid.org/0000-0002-0311-9707
Mario Lebrato 🅭 https://orcid.org/0000-0001-8058-594X
Li-Chun Tseng 🅭 https://orcid.org/0000-0003-0251-565X
Jiang-Shiou Hwang 🅭 https://orcid.org/0000-0003-4881-1163
Dieter Garbe-Schönberg 🅭 https://orcid.org/0000-0001-9006-9463

REFERENCES

Akamatsu, F., Suzuki, Y., Kato, Y., Yoshimizu, C., & Tayasu, I. (2016). A comparison of freeze-drying and oven-drying preparation methods for bulk and compound-specific carbon stable isotope analyses: Examples using the benthic macroinvertebrates Stenopsyche marmorata and Epeorus latifolium. *Rapid Communications in Mass Spectrometry*, 30, 137–142.

Allen, G. J. P., Kuan, P.-L., Tseng, Y.-C., Hwang, P.-P., Quijada-Rodriguez, A. R., & Weihrauch, D. (2020). Specialized adaptations allow vent-endemic crabs (*Xenograpsus testudinatus*) to thrive under extreme environmental hypercapnia. *Scientific Reports*, 10, 11720.

Ashford, O. S., Kenny, A. J., Barrio Froján, C. R. S., Downie, A.-L., Horton, T., & Rogers, A. D. (2019). On the influence of vulnerable marine ecosystem habitats on peracarid crustacean assemblages in the Northwest Atlantic fisheries organisation regulatory area. *Frontiers in Marine Science*, 6. https://doi.org/10.3389/fmars.2019.00401

Bell, J. B., Woulds, C., & Oevelen, D. v. (2017). Hydrothermal activity, functional diversity and chemoautotrophy are major drivers of sea-floor carbon cycling. *Scientific Reports*, 7, 12025.

Carpenter, E. J., Harvey, H. R., Fry, B., & Capone, D. G. (1997). Biogeochemical tracers of the marine cyanobacterium Trichodesmium. *Deep Sea Research Part I: Oceanographic Research Papers*, 44, 27–38.

Chan, B. K. K., Wang, T.-W., Chen, P.-C., Lin, C.-W., Chan, T.-Y., & Tsang, L. M. (2016). Community structure of macrobiota and environmental parameters in shallow water hydrothermal vents off Kueishan Island, Taiwan. *PLoS ONE*, 11, e0148675.

Chang, N.-N., Lin, L.-H., Tu, T.-H., Jeng, M.-S., Chikaraishi, Y., & Wang, P.-L. (2018). Trophic structure and energy flow in a shallow-water hydrothermal vent: Insights from a stable isotope approach. *PLoS ONE*, 13, e0204753.

Chen, C., Chan, T.-Y., & Chan, B. K. K. (2017). *Molluscan diversity in shallow water hydrothermal vents off Kueishan Island, Taiwan*. Marine Biodiversity.

Chen, C.-T. A., Zeng, Z., Kuo, F.-W., Yang, T. F., Wang, B.-J., & Tu, Y.-Y. (2005). Tide-influenced acidic hydrothermal system offshore NE Taiwan. *Chemical Geology, 224*, 69–81.

Cigliano, M., Gambi, M. C., Rodolfo-Metalpa, R., Patti, F. P., & Hall-Spencer, J. M. (2010). Effects of ocean acidification on invertebrate settlement at volcanic CO_2 vents. *Marine Biology, 157*, 2489–2502.

de Ronde, C. E., Baker, E. T., Massoth, G. J., Lupton, J. E., Wright, I. C., Feely, R. A., & Greene, R. R. (2001). Intra-oceanic subduction-related hydrothermal venting, Kermadec volcanic arc, New Zealand. *Earth and Planetary Science Letters, 193*, 359–369.

De Winter, J. C. (2013). *Using the Student's t-test with extremely small sample sizes* (p. 18). Practical Assessment, Research & Evaluation.

Erickson, K. L., Macko, S. A., & Van Dover, C. L. (2009). Evidence for a chemoautotrophically based food web at inactive hydrothermal vents (Manus Basin). *Deep Sea Research Part II: Topical Studies in Oceanography, 56*, 1577–1585.

Fry, B. (1988). Food web structure on Georges Bank from stable C, N, and S isotopic compositions. *Limnology and Oceanography, 33*, 1182–1190.

Fry, B., Gest, H., & Hayes, J. M. (1983). Sulphur isotopic compositions of deep-sea hydrothermal vent animals. *Nature, 306*, 51–52.

Fry, B., Jannasch, H. W., Molyneaux, S. J., Wirsen, C. O., Muramoto, J. A., & King, S. (1991). Stable isotope studies of the carbon, nitrogen and sulfur cycles in the Black Sea and the Cariaco Trench. *Deep Sea Research Part A Oceanographic Research Papers, 38*, S1003–S1019.

Galkin, S. V., & Sagalevich, A. M. (2017). Endemism and biodiversity of hydrothermal vent fauna. In *Extreme biomimetics* (pp. 97–118). Springer.

Gianni, M., Fuller, S. D., Currie, D. E. J., Schleit, K., Goldsworthy, L., & Pike, B. (2016). How much longer will it take? A ten-year review of the implementation of United Nations General Assembly resolutions 61/105, 64/72 and 66/68 on the Management of Bottom Fisheries in Areas Beyond National Jurisdiction: Deep Sea Conservation Coalition.

Hall–Spencer, J., Allain, V., & Fosså, J. H. (2002). Trawling damage to Northeast Atlantic ancient coral reefs. *Proceedings of the Royal Society of London. Series B: Biological Sciences, 269*, 507–511.

Hall-Spencer, J. M., Rodolfo-Metalpa, R., Martin, S., Ransome, E., Fine, M., Turner, S. M., Rowley, S. J., Tedesco, D., & Buia, M.-C. (2008). Volcanic carbon dioxide vents show ecosystem effects of ocean acidification. *Nature, 454*, 96–99.

Harada, Y., Fry, B., Lee, S. Y., Maher, D. T., Sippo, J. Z., & Connolly, R. M. (2020). Stable isotopes indicate ecosystem restructuring following climate-driven mangrove dieback. *Limnology and Oceanography, 65*, 1251–1263.

Ho, T. W., Hwang, J.-S., Cheung, M. K., Kwan, H. S., & Wong, C. K. (2015). Dietary analysis on the shallow-water hydrothermal vent crab *Xenograpsus testudinatus* using Illumina sequencing. *Marine Biology, 162*, 1787–1798.

Hu, M. Y.-A., Hagen, W., Jeng, M.-S., & Saborowski, R. (2012). Metabolic energy demand and food utilization of the hydrothermal vent crab *Xenograpsus testudinatus* (Crustacea: Brachyura). *Aquatic Biology, 15*, 11–25.

Hügler, M., & Sievert, S. M. (2011). Beyond the Calvin cycle: Autotrophic carbon fixation in the ocean. *Annual Review of Marine Science, 3*, 261–289.

Iwaji, I., & Takejiro, O. (1960). Genesis of sulfate in acid hot spring. *Bulletin of the Chemical Society of Japan, 33*, 1018b–1019b.

Jackson, A. L., Inger, R., Parnell, A. C., & Bearhop, S. (2011). Comparing isotopic niche widths among and within communities: SIBER – Stable isotope Bayesian ellipses in R. *Journal of Animal Ecology, 80*, 595–602.

Jeng, M. S., Ng, N. K., & Ng, P. K. (2004). Feeding behaviour: Hydrothermal vent crabs feast on sea 'snow'. *Nature, 432*, 969.

Kharlamenko, V., Zhukova, N., Khotimchenko, S., Svetashev, V., & Kamenev, G. (1995). Fatty-acids as markers of food sources in a shallow-water hydrothermal ecosystem (Kraternaya bight, Yankich Island, Kurile Islands). *Marine Ecology-Progress Series, 120*, 231–241.

Lebrato, M., Wang, Y. V., Tseng, L.-C., Achterberg, E. P., Chen, X.-G., Molinero, J.-C., Bremer, K., Westernströer, U., Söding, E., Dahms, H.-U., Küter, M., Heinath, V., Jöhnck, J., Konstantinou, K. I., Yang, Y. J., Hwang, J.-S., & Garbe-Schönberg, D. (2019). Earthquake and typhoon trigger unprecedented transient shifts in shallow hydrothermal vents biogeochemistry. *Scientific Reports, 9*, 16926.

Ledger, M. E., Brown, L. E., Edwards, F. K., Hudson, L. N., Milner, A. M., & Woodward, G. (2013). Chapter six - extreme climatic events Alter aquatic food webs: A synthesis of evidence from a mesocosm drought experiment. In G. Woodward & E. J. O'Gorman (Eds.), *Advances in ecological research* (pp. 343–395). Academic Press.

Levin, L. A., Baco, A. R., Bowden, D. A., Colaco, A., Cordes, E. E., Cunha, M. R., Demopoulos, A. W. J., Gobin, J., Grupe, B. M., Le, J., Metaxas, A., Netburn, A. N., Rouse, G. W., Thurber, A. R., Tunnicliffe, V., Van Dover, C. L., Vanreusel, A., & Watling, L. (2016). Hydrothermal vents and methane seeps: Rethinking the sphere of influence. *Frontiers in Marine Science, 3*. https://doi.org/10.3389/fmars.2016.00072

Little, C. T. S., & Vrijenhoek, R. C. (2003). Are hydrothermal vent animals living fossils? *Trends in Ecology & Evolution, 18*, 582–588.

Luther, G. W., Rozan, T. F., Taillefert, M., Nuzzio, D. B., Di Meo, C., Shank, T. M., Lutz, R. A., & Cary, S. C. (2001). Chemical speciation drives hydrothermal vent ecology. *Nature, 410*, 813–816.

Martin, W., Baross, J., Kelley, D., & Russell, M. J. (2008). Hydrothermal vents and the origin of life. *Nature Reviews Microbiology, 6*, 805–814.

McCutchan, J. H., Jr., Lewis, W. M., Jr., Kendall, C., & McGrath, C. C. (2003). Variation in trophic shift for stable isotope ratios of carbon, nitrogen, and sulfur. *Oikos, 102*, 378–390.

Michel, L. N., Bell, J. B., Dubois, S. F., Le Pans, M., Lepoint, G., Olu, K., Reid, W. D. K., Sarrazin, J., Schaal, G., & Hayden, B. (2021). *DeepIso - a global open database of stable isotope ratios and elemental contents for deep-sea ecosystems*. SEANOE.

Minagawa, M., & Wada, E. (1986). Nitrogen isotope ratios of red tide organisms in the East China Sea: A characterization of biological nitrogen fixation. *Marine Chemistry, 19*, 245–259.

Minic, Z. (2009). Organisms of deep sea hydrothermal vents as a source for studying adaptation and evolution. *Symbiosis, 47*, 121–132.

Miyake, H., Oda, A., Wada, S., Kodaka, T., & Kurosawa, S. (2019). First record of a shallow hydrothermal vent crab. *Xenograpsus Testudinatus, from Shikine-Jima Island in the Izu Archipelago, 21*, 31–36.

Ng, N. K., Huang, J.-F., & Ho, P.-H. (2000). Description of a new species of hydrothermal crab, *Xenograpsus testudinatus* (Crustacea: Decapoda: Brachyur a: Grapsidae) from Taiwan. *National Taiwan Museum Special Publication Series, 10*, 191–199.

Oana, S., & Ishikawa, H. (1966). Sulfur isotopic fractionation between sulfur and sulfuric acid in the hydrothermal solution of sulfur dioxide. *Geochemical Journal, 1*, 45–50.

Petersen, J. M., Zielinski, F. U., Pape, T., Seifert, R., Moraru, C., Amann, R., Hourdez, S., Girguis, P. R., Wankel, S. D., Barbe, V., Pelletier, E., Fink, D., Borowski, C., Bach, W., & Dubilier, N. (2011). Hydrogen is an energy source for hydrothermal vent symbioses. *Nature, 476*, 176–180.

Ponsard, J., Cambon-Bonavita, M.-A., Zbinden, M., Lepoint, G., Joassin, A., Corbari, L., Shillito, B., Durand, L., Cueff-Gauchard, V., & Compère, P. (2013). Inorganic carbon fixation by chemosynthetic ectosymbionts and nutritional transfers to the hydrothermal vent host-shrimp Rimicaris exoculata. *The ISME Journal, 7*, 96–109.

Portail, M., Olu, K., Dubois, S. F., Escobar-Briones, E., Gelinas, Y., Menot, L., & Sarrazin, J. (2016). Food-web complexity in Guaymas basin hydrothermal vents and cold seeps. *PLoS ONE, 11*, e0162263.

Post, D. M. (2002). Using stable isotopes to estimate trophic position: Models, methods, and assumptions. *Ecology, 83*, 703–718.

R Core Team. (2020). *R: A language and environment for statistical computing*. R Foundation for Statistical Computing.

Ramirez-Llodra, E., Tyler, P. A., Baker, M. C., Bergstad, O. A., Clark, M. R., Escobar, E., Levin, L. A., Menot, L., Rowden, A. A., Smith, C. R., & Van Dover, C. L. (2011). Man and the last great wilderness: Human impact on the Deep Sea. *PLoS ONE*, *6*, e22588.

Rees, A. P. (2012). Pressures on the marine environment and the changing climate of ocean biogeochemistry. *Philosophical Transactions of the Royal Society A: Mathematical, Physical and Engineering Sciences*, *370*, 5613–5635.

Reid, W. D. K., Sweeting, C. J., Wigham, B. D., Zwirglmaier, K., Hawkes, J. A., McGill, R. A. R., Linse, K., & Polunin, N. V. C. (2013). Spatial differences in east scotia ridge hydrothermal vent food webs: Influences of chemistry, microbiology and predation on trophodynamics. *PLoS ONE*, *8*, e65553.

Sagarin, R., Adams, J., Blanchette, C., Brusca, R., Chorover, J., Cole, J., Micheli, F., Munguia-Vega, A., Rochman, C., Bonine, K., van Haren, J., & Troch, P. (2016). Between control and complexity: Opportunities and challenges for marine mesocosms. *Frontiers in Ecology and the Environment*, *14*, 389–396.

Sakai, H. (1968). Isotopic properties of sulfur compounds in hydrothermal processes. *Geochemical Journal*, *2*, 29–49.

Sellanes, J., Zapata-Hernández, G., Pantoja, S., & Jessen, G. L. (2011). Chemosynthetic trophic support for the benthic community at an intertidal cold seep site at Mocha Island off Central Chile. *Estuarine, Coastal and Shelf Science*, *95*, 431–439.

Shiozaki, T., Takeda, S., Itoh, S., Kodama, T., Liu, X., Hashihama, F., & Furuya, K. (2015). Why is *Trichodesmium* abundant in the Kuroshio? *Biogeosciences*, *12*, 6931–6943.

Suzuki, K., Yoshida, K., Watanabe, H., & Yamamoto, H. (2018). Mapping the resilience of chemosynthetic communities in hydrothermal vent fields. *Scientific Reports*, *8*, 9364.

Svensson, E., Schouten, S., Hopmans, E. C., Middelburg, J. J., & Damste, J. S. S. (2016). Factors controlling the stable nitrogen isotopic composition (δ^{15}N) of lipids in marine animals. *PLoS ONE*, *11*, e0146321.

Tang, K. H., & Blankenship, R. E. (2010). Both forward and reverse TCA cycles operate in green sulfur bacteria. *The Journal of Biological Chemistry*, *285*, 35848–35854.

Tarasov, V. G., Gebruk, A. V., Mironov, A. N., & Moskalev, L. I. (2005). Deep-sea and shallow-water hydrothermal vent communities: Two different phenomena? *Chemical Geology*, *224*, 5–39.

Ueda, A., Sakai, H., & Sasaki, A. (1979). Isotopic composition of volcanic native sulfur from Japan. *Geochemical Journal*, *13*, 269–275.

Wada, E., & Hattori, A. (1976). Natural abundance of 15N in particulate organic matter in the North Pacific Ocean. *Geochimica et Cosmochimica Acta*, *40*, 249–251.

Wang, L., Cheung, M. K., Kwan, H. S., Hwang, J. S., & Wong, C. K. (2015). Microbial diversity in shallow-water hydrothermal sediments of Kueishan Island, Taiwan as revealed by pyrosequencing. *Journal of Basic Microbiology*, *55*, 1308–1318.

Wang, T.-W., Chan, T.-Y., & Chan, B. K. K. (2014). Trophic relationships of hydrothermal vent and non-vent communities in the upper sublittoral and upper bathyal zones off Kueishan Island, Taiwan: A combined morphological, gut content analysis and stable isotope approach. *Marine Biology*, *161*, 2447–2463.

Wang, T.-W., Lau, D. C. P., Chan, T.-Y., & Chan, B. K. K. (2022). Autochthony and isotopic niches of benthic fauna at shallow-water hydrothermal vents. *Scientific Reports*, *12*, 6248.

Wang, V. Y., Larsen, T., Lebrato, M., Tseng, L.-C., Lee, P.-W., Sánchez, N., Molinero, J.-C., Hwang, J.-S., Chan, T.-Y., & Garbe-Schönberg, D. (2023). Supplementary Data to "Foraging under extreme events: Contrasting adaptations by benthic macrofauna to drastic biogeochemical disturbance". *Functional Ecology*. https://doi.org/10.5281/zenodo.7680525

Wang, X., Li, C., Wang, M., & Zheng, P. (2018). Stable isotope signatures and nutritional sources of some dominant species from the PACManus hydrothermal area and the Desmos caldera. *PLoS ONE*, *13*, e0208887.

Weltje, G. J. (1997). End-member modeling of compositional data: Numerical-statistical algorithms for solving the explicit mixing problem. *Mathematical Geology*, *29*, 503–549.

Wickham, H. (2016). *ggplot2: Elegant graphics for data analysis*. Springer-Verlag.

Wu, C., Fu, F.-X., Sun, J., Thangaraj, S., & Pujari, L. (2018). Nitrogen fixation by Trichodesmium and unicellular diazotrophs in the northern South China Sea and the Kuroshio in summer. *Scientific Reports*, *8*, 2415.

Wu, J.-Y., Lin, S.-Y., Peng, S.-H., Hung, J.-J., Arthur Chen, C.-T., & Liu, L.-L. (2021). Isotopic niche differentiation in benthic consumers from shallow-water hydrothermal vents and nearby non-vent rocky reefs in northeastern Taiwan. *Progress in Oceanography*, *195*, 102596.

Wu, X., Wu, B., Song, J., & Li, X. (2014). Spatio-temporal distribution of dissolved sulfide in China marginal seas. *Chinese Journal of Oceanology and Limnology*, *32*, 1145–1156.

Yadav, S., Prajapati, R., & Atri, N. (2016). Effects of UV-B and heavy metals on nitrogen and phosphorus metabolism in three cyanobacteria. *Journal of Basic Microbiology*, *56*, 2–13.

Yang, S.-H., Chiang, P.-W., Hsu, T.-C., Kao, S.-J., & Tang, S.-L. (2016). Bacterial community associated with organs of shallow hydrothermal vent crab *Xenograpsus testudinatus* near Kuishan Island, Taiwan. *PLoS ONE*, *11*, e0150597.

SUPPORTING INFORMATION

Additional supporting information can be found online in the Supporting Information section at the end of this article.

Supplementary Text I. Background of the study region.

Supplementary Text II. Extreme impact of Earthquake and Typhoon in KST vents in 2016.

Supplementary Text III. Will Oven-dry and freeze-dry procedures affect the stable isotope values of our macroinvertebrate samples?

Supplementary Video S1. Turtle Island live earthquake video recorded by Taiwan TV.

Supplementary Video S2. KST ocean conditions during and after C5 typhoon Nepartak in 2016.

Supplementary Video S3. Turtle Island shallow vents changes from 2001 to 2017.

Supplementary Table S1. Individual δ^{13}C, δ^{15}N and δ^{34}S values and shell width of individual organisms from the KST vent.

Supplementary Table S2. Individual δ^{13}C, δ^{15}N and δ^{34}S values of several potential food sources at the KST region.

Supplementary Table S3. MANOVA and ANOVA results comparing δ^{13}C, δ^{15}N, δ^{34}S values between the *Xenograpsus testudinatus* collected in the Yellow and White Vents in 2018.

Supplementary Table S4. MANOVA and ANOVA results comparing δ^{13}C, δ^{15}N, δ^{34}S values between the male and female *Xenograpsus testudinatus* in 2018.

Supplementary Table S5. MANOVA and ANOVA results comparing δ^{13}C, δ^{15}N, δ^{34}S values between 2015 and 2018 for vent crab (*Xenograpsus testudinatus*).

Supplementary Table S6. Summary of Welch Two Sample t-test comparing δ^{13}C, δ^{15}N, δ^{34}S values between the vent crab (*Xenograpsus testudinatus*) and pooled Mollusca group (*Ergalatax contracta, Thylacodes adamsii, Bostrycapulus gravispinosus*) in 2017. Lower and upper limits of 95% Confidence Intervals (CI) are also presented.

Supplementary Table S7. MANOVA and ANOVA results comparing δ^{13}C, δ^{15}N, δ^{34}S values between the vent crab (*Xenograpsus testudinatus*) and pooled Mollusca group (*Ergalatax contracta, Thylacodes adamsii, Bostrycapulus gravispinosus*) in 2015.

Supplementary Table S8. MANOVA and ANOVA results comparing δ^{13}C, δ^{34}S values between the vent crab (*Xenograpsus testudinatus*) and pooled Mollusca group (*Ergalatax contracta, Thylacodes adamsii, Bostrycapulus gravispinosus*) in 2018.

Supplementary Table S9. The δ^{13}C, δ^{15}N, and δ^{34}S niche space for all organisms. TA stands for total community area, SEA stands for Standard Ellipse Area, and SEAc stands for Standard Ellipse Area corrected for small sample size.

Supplementary Fig. S1. Underwater image next to the new Yellow Vent mouths (121.962°E, 24.834°N) to monitor the vent crab (*Xenograpsus testudinatus*) population change.

Supplementary Fig. S2. Inter-annual δ^{34}S, δ^{13}C and δ^{15}N variability of benthic organism tissues in the Kuishantao Island in 2015 and 2018.

Supplementary Fig. S3. The isotope mixing space defined by the sampled food sources.

Supplementary Discussion I. Why Bayesian mixing model is an inappropriate approach in our study?